

S.K. BARAL¹, M.M. THAWRE², B.R. SUNIL³, RAVIKUMAR DUMPALA^{1*}

EFFECT OF BURNISHING LOAD ON SURFACE ROUGHNESS AND WEAR BEHAVIOUR OF ZE41 MAGNESIUM ALLOY

Magnesium (Mg) alloys have become an attractive choice for lightweight structural applications. However, improving the tribological characteristics of Mg alloys is essential to widen the range of applications. In the present work, ball burnishing was performed with different burnishing loads from 40 N to 80 N to investigate its effect on surface roughness, microhardness, and wear resistance. It was found that the 50 N burnishing load exhibits the best surface finish with a reduction of 46.2% in surface roughness compared to unburnished alloy. The highest microhardness was observed at 60 N load with an improvement of ~35.5%. Higher loads beyond 50 N resulted in increased surface roughness. Higher burnishing load caused surface distortion and flaking which decreased the microhardness beyond 60 N load. At 50 N burnishing load, better wear resistance with a reduction of ~40% was achieved compared to unburnished alloy. Improvement in surface finish and microhardness are responsible for better wear resistance. Worn surfaces exhibited abrasion, oxidation, and delamination wear mechanisms in the unburnished sample. Whereas, delamination wear was absent in the burnished specimen at 50 N burnishing load.

Keywords: ZE41 magnesium alloy; Burnishing load; Surface roughness; Microhardness; Wear resistance

1. Introduction

Recently, magnesium (Mg) alloys demonstrated their potential as promising candidates to manufacture light weight structures in aviation, defence, electronics and automobile industries due to lower density, higher specific strength, and adequate castability [1-4]. Along with the mechanical performance, exhibiting adequate wear and frictional characteristics is also crucial in engineering applications to tailor Mg alloys for wide range of usage. Lower hardness and poor corrosion and wear resistance of Mg alloys are responsible for its limited use in engineering fields [5]. To overcome these limitations, developing Mg based new alloys has become an active research field in materials engineering [1,2]. On the other hand, several processing techniques have been applied to improve the properties of Mg alloys by either significantly changing the microstructure or chemical composition of the alloys. Some of these techniques involve modification of surface properties without affecting the bulk microstructure and chemical composition of Mg alloys which can be categorized as surface engineering techniques. Among these methods, ball burnishing is one of the alternatives that

uses a spherical ball to press as well as to roll on the substrate surface and results in good surface quality, improved hardness and imparts compressive residual stresses at the surface [6]. The ball burnishing process is a solid state surface treatment which is simple and can be conveniently carried out with the existing machine tools. For example, conventional or CNC turning and vertical milling machines can be used for performing ball burnishing operations without employing high-cost specially designed equipment [7]. From the literature, it can be learned that several Mg alloys have been subjected to ball burnishing to improve their surface properties.

Salahshoor et al. conducted ball burnishing of Mg-Ca alloy with operation parameters including pressure, speed, feed, number of paths, etc. It was observed from the demonstrated results that the burnished surfaces were smoother and shiny. Furthermore, subsurface hardness was improved with burnishing pressure, and also residual stresses were found to be highly compressive after burnishing [8]. In addition to imparting the residual stresses, ball burnishing process also introduce microstructural changes by producing twins and sub grains. Uddin et al. ball-burnished AZ31B Mg alloy that resulted in smooth surface topography, improved

¹ DEPARTMENT OF MECHANICAL ENGINEERING, VISVESVARAYA NATIONAL INSTITUTE OF TECHNOLOGY, NAGPUR 440010, INDIA

² DEPARTMENT OF METALLURGICAL AND MATERIALS ENGINEERING, VISVESVARAYA NATIONAL INSTITUTE OF TECHNOLOGY, NAGPUR 440010, INDIA

³ DEPARTMENT OF MECHANICAL ENGINEERING, COLLEGE OF ENGINEERING, PRINCE MOHAMMAD BIN FAHD UNIVERSITY, AL-KHOBAR 31952, SAUDI ARABIA

* Corresponding author: ravikumardumpala@mec.vnit.ac.in



hardness, and microstructural disturbances with the formation of deformation twins [9]. Jagadeesh et al. processed ZE41 Mg alloy at varying burnishing parameters. The study showed a 94.9% and 50.62% improvement in surface finish and microhardness respectively. The reason behind the significant improvement in hardness was claimed to the effect of strain hardening achieved in the substrate after burnishing [10]. Thus, it was evident from literature that ball burnishing improves surface finish and microhardness. The tribological performance evaluation after ball burnishing of ZE41 alloy demonstrates that the wear rate and coefficient of friction (COF) are decreased by 51.22% and 72.58%, respectively. The improved wear resistance is ascribed to the enhancement in surface finish and hardness due to strain hardening. Worn surface shows oxidation, delamination and plastic deformation as dominant wear mechanisms [11]. An optimum burnishing condition was decided by investigation on ZE41 alloy that resulted in a decreased wear rate of 40% and COF of 45%. Furthermore, a wear-burnishing map was constructed that shows different wear mechanisms seen at different levels of wear regimes [12].

From the literature, it is understood that the role of ball burnishing of Mg alloys on friction and wear performance is not sufficiently explored, in particular for ZE41 alloy. Therefore, in the present study, ball burnishing was performed with varying loads to investigate its effect on surface roughness, microhardness, friction, and wear characteristics and further the corresponding wear mechanisms were explored.

2. Experimental details

Rare earth (RE) ZE41 Mg alloy in as-cast condition was used with a chemical composition (by weight) of 3.90% zinc (Zn), 0.54% cerium (Ce), 0.54% zirconium (Zr), total RE 1.10%, and balance is Mg. The received alloy was cut by a power hacksaw and the surface was milled using a CNC milling machine. Samples of size $20 \times 20 \times 5 \text{ mm}^3$ were cut from the machined plates. Burnishing operation was performed on a 3-axis CNC milling machine (MTAB, MAXMILL) using a burnishing tool that has a freely rotating spherical tungsten carbide ball of 10 mm

diameter supported by three smaller balls. The required burnishing load was applied by elastically compressing the spring. The ball rotates as well as slides simultaneously on the surface of the workpiece during the process. Burnishing was performed with varying loads from 40 N to 80 N. The other burnishing parameters are shown in TABLE 1 [10,11].

TABLE 1

Ball Burnishing process parameters

Burnishing Speed (RPM)	Feed rate (mm/min)	Number of passes	Lateral feed (micron)	Burnishing load (N)
1200	150	1	50	40, 50, 60, 70, 80

A stereo zoom microscope (RSM-9, Radical) was used to capture the pictures of burnished area. The roughness of each sample surface was assessed by using a surface profile meter (Mitutoyo, SJ-410). The microhardness of specimen was measured by Vickers microhardness setup (Economet VH1-MDX, Chennai Metco) using a load of 50 g and 15 s dwell time.

Wear properties were assessed by conducting sliding wear test in dry condition by using a reciprocating type tribometer (Ducom India) against a steel ball ($\Phi 6 \text{ mm}$) having 62 HRC hardness. Milled and burnished samples were cleaned, dried and weights were recorded by using a digital balance of precision 0.1 mg. The wear test was conducted using a 10 N normal load, 0.06 m/s sliding speed, and 100 m travelling distance. A stroke length of 6 mm and frequency of 5 Hz was used. The recorded friction coefficient values were against time. After the completion of test, the weight of worn specimens was taken and volume wear loss was determined. Thereafter, the specific wear rate (mm^3/Nm) was determined using the formula in Eq. (1).

$$\text{Specific wear rate } \left(\text{mm}^3/\text{Nm} \right) = \frac{\text{Volume wear loss}}{\text{sliding distance} \times \text{normal load}} \quad (1)$$

Where *Volume wear loss* is in mm^3 , *sliding distance* is in meter (m) and *normal load* is in newton (N).

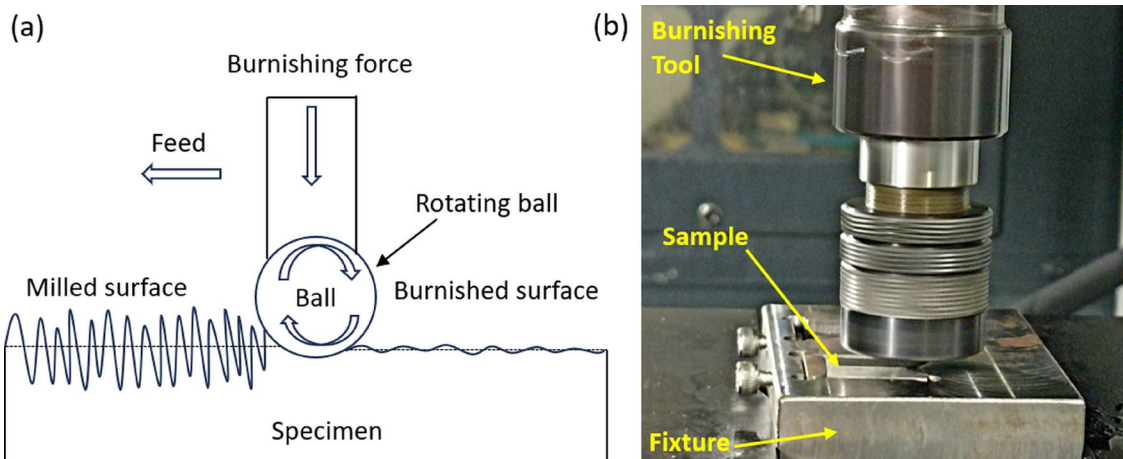


Fig. 1. (a) Schematic of ball burnishing process, and (b) photograph showing the burnishing process setup

The worn surfaces of the specimen and debris were examined by a “scanning electron microscope” (SEM, JEOL JSM-6380A), and “energy dispersive spectroscopy” (EDS), and the corresponding wear mechanisms were evaluated.

3. Results and discussion

3.1. Surface roughness and microhardness

The surface features of unburnished and burnished samples with different loads are shown in Fig. 2. The pictures give an insight into understanding the mechanism of ball burnishing. Fig. 2(a) shows milling marks that appeared in the unburnished specimen. Fig. 2(b) to 2(f) shows surface features under burnishing loads varied from 40 N to 80 N respectively. A roughness of $0.894\ \mu\text{m}$ was measured at the surface of the base alloy. Fig. 3(a) shows surface roughness variations with different burnishing loads. With the increased load from 50 N to 80 N, increased

roughness was noticed. At 50 N, the surface roughness value was minimum and the 40 N load resulted in higher surface roughness compared to 50 N load. It is noted that a lower burnishing load resulted in a better surface finish, but lower than 50 N load is not sufficient to deform the surface ridges and asperities and partial deformation of asperities in 40N load resulted in degraded surface quality and surface roughness is high [10]. As the load increases beyond 50 N load the surface finish gradually decreases. But 60 N and 70 N burnishing load exhibited better surface finish compared to the unburnished specimen. At 80 N burnishing load, the surface shows flaking and distortion and has the highest surface roughness.

At lower load (40 N), the burnishing ball penetration into the workpiece surface is smaller that resulted in lower level of deformation in the surface asperities and led to poor surface finish. At higher load (50 N), the contact area of the rotating ball is also increased, that widens the area of plastic deformation resulting in complete deformation of the surface asperities to improve the surface finish [10]. However, further increase in

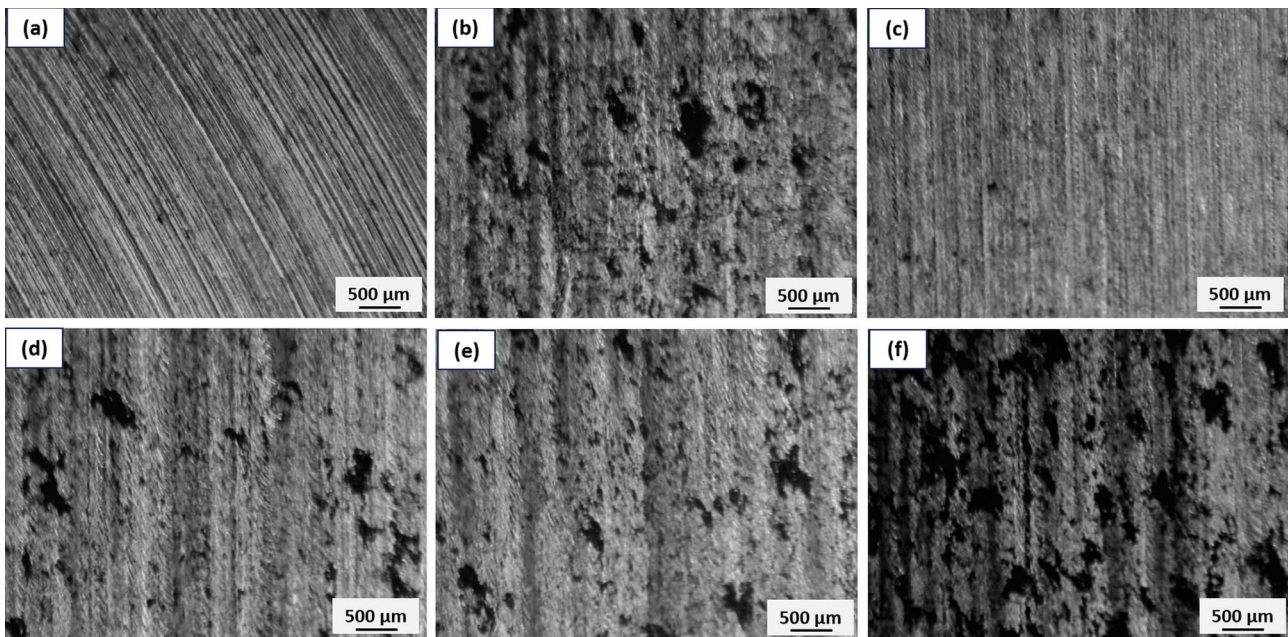


Fig. 2. Surface features of (a) milled surface, and burnished surfaces with loads (b) 40 N, (c) 50 N, (d) 60 N, (e) 70 N, (f) 80 N

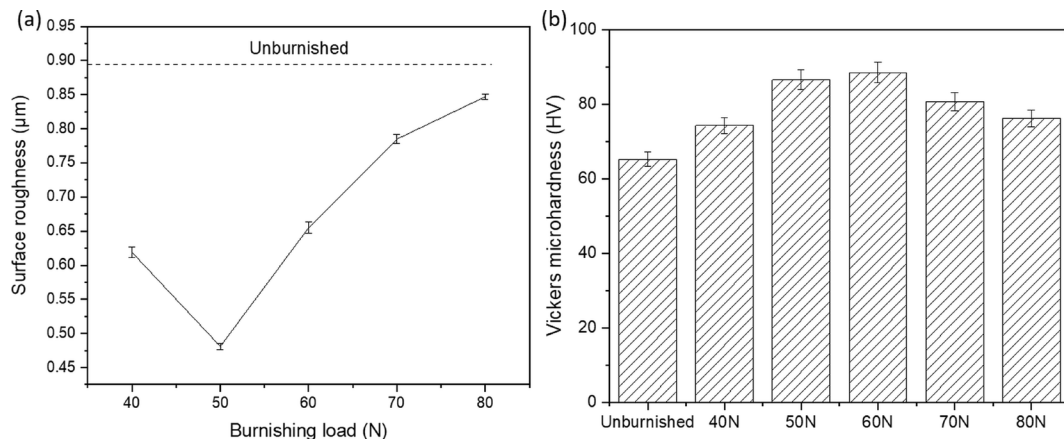


Fig. 3. Plot of (a) surface roughness vs. burnishing load, and (b) microhardness vs. burnishing load

burnishing load causes gradual flaking and distortion of surfaces that increased the surface roughness [11]. At 80 N load the surface flaking and distortion are high because of excessive strain hardening. 50 N burnishing load produced minimum surface roughness of 0.481 μm which is a reduction of 46.2% compared to the unburnished specimen. Increased surface roughness of 0.847 μm was measured in case of 80 N load.

The plot of Vickers microhardness against burnishing loads is shown in Fig. 3(b). It was noticed that microhardness has been increased with burnishing load from 40 N to 60 N, thereafter it was decreased up to 80 N. Burnishing load of 60 N resulted in the highest microhardness (88.5 HV) with a 35.5% improvement compared to the unburnished specimen (65.3 HV). The surface produced with 50 N burnishing load has 86.6 HV hardness with a 32.6% increment compared to unburnished alloy. At lower burnishing load, the plastic deformation is not sufficient, and partial deformation of surface causes lower strain hardening. At higher load, the surface deformation increased thereby the intensity of strain hardening increased and microhardness was also improved as observed at 50 N and 60 N load [11, 13]. However, beyond 60 N load, the microhardness was decreased due to the flaking and distortion caused by severe plastic deformation and excessive strain hardening of surface as observed at 80 N burnishing load [10].

3.2. Wear behaviour

3.2.1. Friction coefficient and wear rate

The COF curves for unburnished and burnished specimens with burnishing loads (40 N to 80 N) are presented in Fig. 4(a). The unburnished specimen shows a higher friction coefficient at the beginning due to the presence of sharp ridges and initial surface asperities of counter ball. Once the initial surface asperities were deformed, the COF was gradually decreased. Mg alloy is always prone to oxidation at air environment [14,15]. The counter ball was continuously sliding against the magnesium specimen due to which frictional heat was produced

that oxidized the substrate surface [16]. This oxide film acts as a temporary protective layer that reduces material loss and the COF is reduced [17]. However, with the passage of time, the oxide layers became unstable and continuously formed and removed under the repeated sliding action of steel ball. This resulted in the fluctuation of the COF curve and increased the COF [18]. An average COF of 0.26 was measured in the case of unburnished specimen.

From Fig. 4(a), higher COF can be noticed for the burnished surfaces at the beginning of the sliding due to the initial asperities on the surface of the counter ball. However, due to the improved hardness and surface finish of the substrate, the COF curve gradually became stable. Further, the developed oxide layers were stable for a longer time compared to the unburnished sample. However, gradually the repeated formation and removal of oxide layers due to sliding action of counter ball caused fluctuations in the COF curves. The 50 N burnishing load resulted in the lowest COF of 0.15 due to the improved hardness and best surface finish. All the burnished samples exhibited lower COF compared to unburnished. The average COF at 40 N, 50 N, 60 N, 70 N, and 80 N burnishing loads was measured as 0.18, 0.15, 0.17, 0.19, and 0.20. Improved hardness of surface and production of better surface quality due to the ball burnishing are responsible for lower COF.

Fig. 4(b) represents the wear rate of unburnished and burnished samples. The unburnished sample exhibits the highest wear rate of $5.75 \times 10^{-4} \text{ mm}^3/\text{Nm}$. This is due to the lower hardness and surface finish, and removal of more amount of material under sliding force of counter ball. The burnished samples with improved microhardness provide sufficient resistance against the counter ball and the material removal is lowered. 50 N load exhibits a lower wear rate of $3.45 \times 10^{-4} \text{ mm}^3/\text{Nm}$ with a reduction of 40% compared to unburnished sample. With increased burnishing load beyond 50 N, the wear rate was also increased. At 80 N burnishing load, a wear rate of $5.19 \times 10^{-4} \text{ mm}^3/\text{Nm}$ was measured which is the highest wear rate among all the burnished alloys. The presence of flaking and surface distortions due to excessive strain hardening are responsible for the higher removal of material at 80 N load.

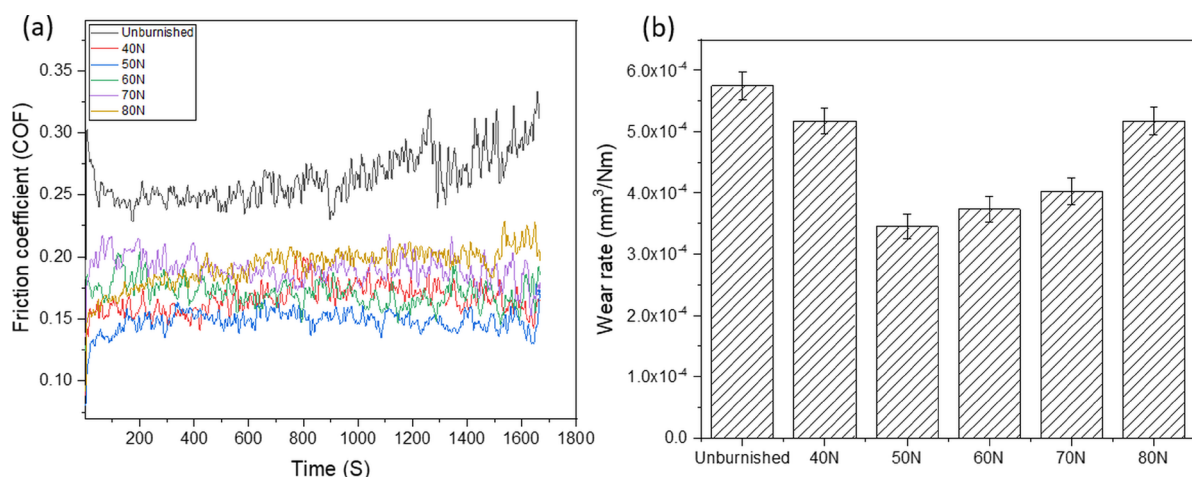


Fig. 4. (a) Friction coefficient curve and (b) wear rate plot for unburnished and burnished samples

3.2.2. Worn surface morphology

Fig. 5(a-f) depicts worn surfaces and wear tracks of unburnished and burnished samples with different loads. It was observed that the unburnished alloy has a bigger wear track width of 1.68 ± 0.03 mm and all other burnished samples resulted in a smaller track width. Improved hardness and higher surface finish are responsible for lower penetration of the ball and thus width of the track was decreased. At 50 N burnishing load, the sample shows least wear track width of 1.31 ± 0.01 mm and with the increased burnishing load beyond 50 N, wear track width was

increased. 80 N burnishing load showed the highest track width among burnished samples due to the presence of flaking and surface defects, which were responsible for lower resistance to counter ball and higher amount of material is removed.

The worn surface morphologies of unburnished and burnished samples at 50 N load from SEM analysis are compared in Fig. 6(a, b) and Fig. 6(d, e), respectively. Longer and relatively finer grooves were observed on the surface of base alloy aligned in the direction of the sliding (Fig. 6(a)), which were produced due to the abrasive action of the hard particles present in the counter ball [19,20]. Oxide debris were visible all over the worn

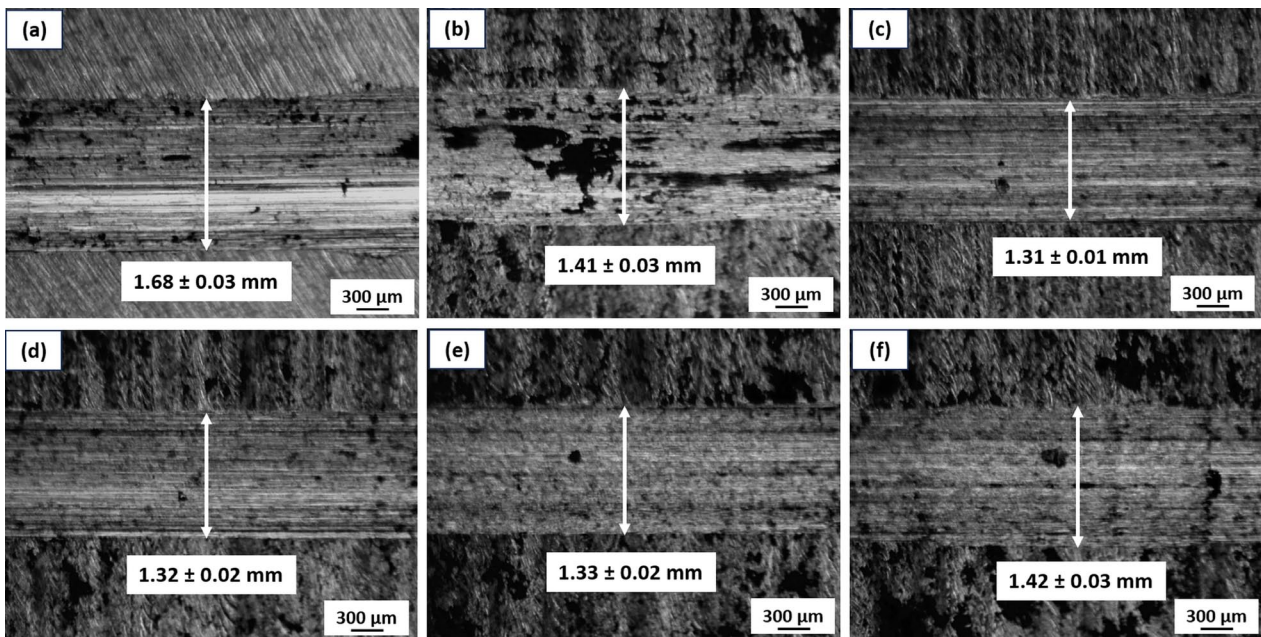


Fig. 5. Wear tracks of (a) unburnished sample, and burnished samples with loads (b) 40 N, (c) 50 N, (d) 60 N, (e) 70 N, (f) 80 N

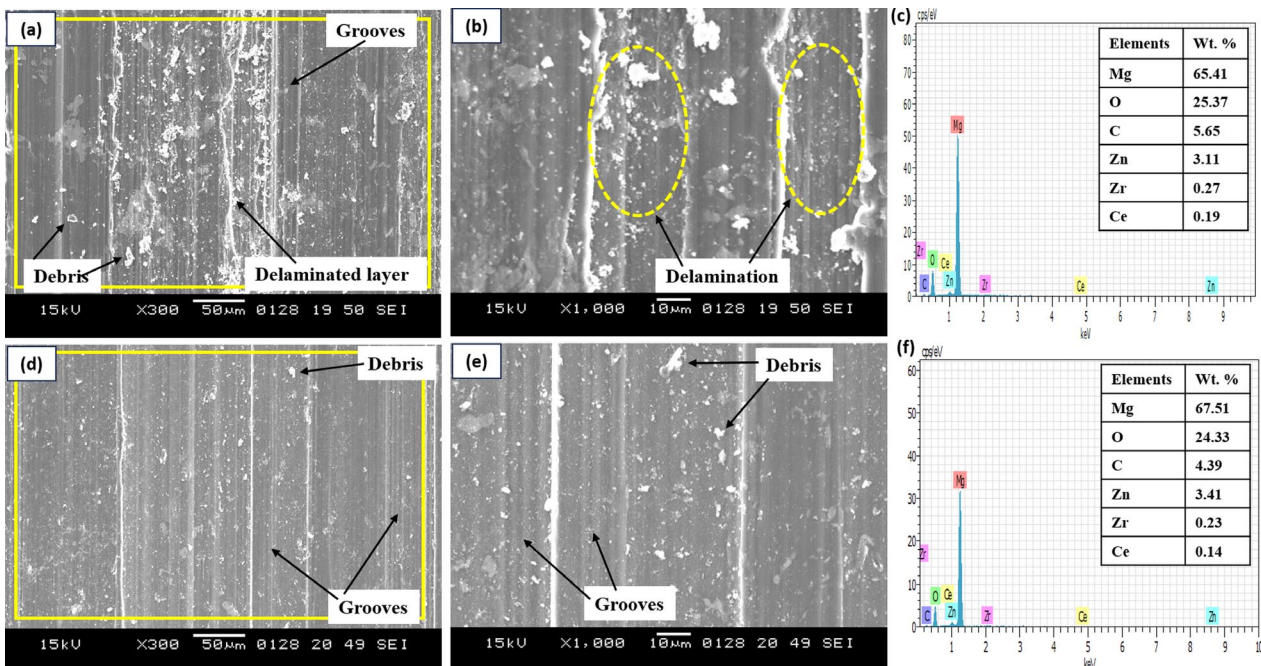


Fig. 6. Worn surface morphology of (a, b) unburnished sample and (d, e) burnished sample at 50 N load. EDS analysis of (c) unburnished sample, and (f) burnished sample at 50 N load

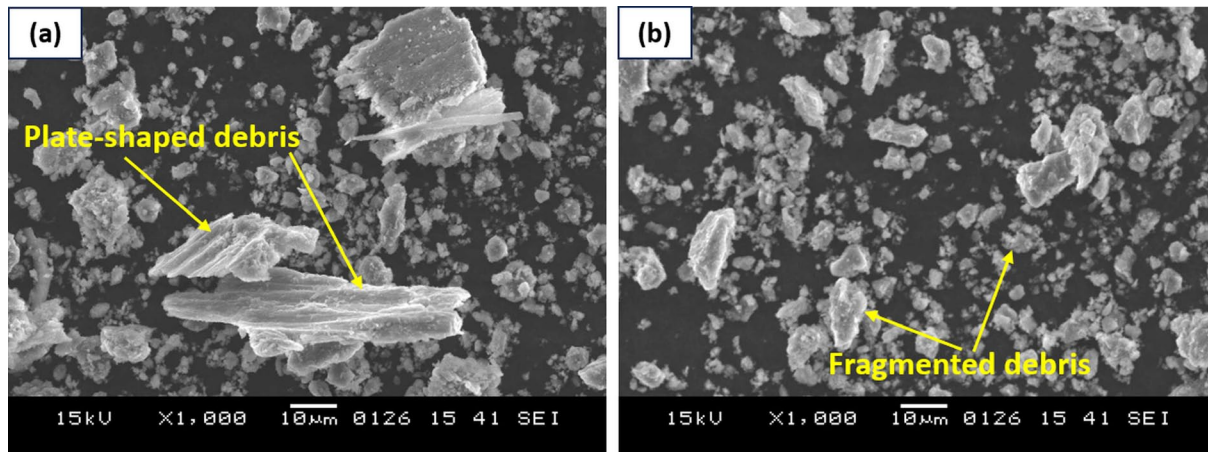


Fig. 7. Collected wear debris morphology of (a) unburnished sample, and (b) burnished sample at 50 N load

surface of unburnished alloy and EDS analysis shows higher percentage of oxygen that confirms oxidation wear in Fig. 6(c) [21,22]. Frictional heating during reciprocating action of counter ball is responsible for oxidation of substrate surface which led to formation of oxide debris. Delaminated layers were observed in unburnished worn surface. During the wear process the sub-surface cracks grow and propagate underneath and when these cracks join the wear surface delamination happens [23,24]. Long plate-shaped wear debris were produced due to the delamination as shown in Fig. 7(a) [25].

However, delamination is not observed in the case of 50 N burnished sample as presented in Fig. 6(d, e). Numerous parallel grooves due to abrasion wear were noticed [26]. Smaller oxide debris all over the worn surface were observed and corresponding EDS analysis of Fig. 6(d) shows higher percentage of oxygen indicating oxidation wear. In Fig. 7(b), the debris morphology shows small fragment shape indicating abrasion wear [27]. Hence from the present study, it can be understood that the abrasion wear coupled with oxidation and delamination wear mechanisms are observed as prominent in the unburnished specimen. Whereas no sign of delamination was observed in the burnished sample.

4. Conclusion

In the current study, ball burnishing of ZE41 magnesium alloy with burnishing loads from 40 N to 80 N was performed, and its effect on surface roughness, microhardness and wear was examined. It was observed that ball burnishing produced better surface finish by deforming the surface asperities. The 50 N burnishing load produced best surface finish with a reduction in surface roughness by 46.2% compared to unburnished alloy. Plastic deformation and subsequent strain hardening were responsible for improved microhardness in the burnished samples. At 60 N load the highest microhardness with an improvement of 35.5% compared to unburnished sample was observed. However, higher burnishing load caused surface distortion and flaking due to excessive strain hardening and reduced hardness. The COF and wear rate of burnished samples were low compared to un-

burnished. The 50 N burnished sample exhibited minimum wear rate with a reduction of 40% compared to unburnished alloy. Improved hardness due to strain hardening and better surface finish are responsible for lower material removal. Abrasion wear coupled with oxidation and delamination wear mechanisms are found to be dominant in unburnished alloy, whereas in the case of burnished specimens, abrasion and oxidation mechanisms played dominant role.

REFERENCES

- [1] T. Xu, Y. Yang, X. Peng, J. Song, F. Pan, Overview of advancement and development trend on magnesium alloy. *J. Magnesium Alloys* **7**, 536-544 (2019). DOI: <https://doi.org/10.1016/j.jma.2019.08.001>
- [2] B.L. Mordike, T. Ebert, Magnesium: Properties – applications – potential. *Mater. Sci. Eng. A* **302**, 37-45 (2001). DOI: [https://doi.org/10.1016/S0921-5093\(00\)01351-4](https://doi.org/10.1016/S0921-5093(00)01351-4)
- [3] Y.-C. Shin, S.-H. Ha, A.W. Shah, Effects of SPD by Biaxial Alternating Forging on the Tensile Properties and Microstructure of AZ31B Magnesium Alloy. *Arch. Metall. Mater.* **68**, 97-101 (2023). DOI: <https://doi.org/10.24425/amm.2023.141479>
- [4] L. Elen, Y. Turen, H. Ahlatci, Y. Sun, M. Unal, Investigation of Microstructure, Mechanical and Corrosion Properties of Biodegradable Mg-Ag Alloys. *Arch. Metall. Mater.* **67**, 889-900 (2022). DOI: <https://doi.org/10.24425/amm.2022.139680>
- [5] X. Chen, X. Xie, Y. Zhang, H. Wang, Z. Liang, Tungsten carbide coating prepared by ultrasonic shot peening to improve the wear properties of magnesium alloys. *J. Mater. Res. Technol.* **26**, 2451-2464 (2023). DOI: <https://doi.org/10.1016/j.jmrt.2023.08.079>
- [6] S.K. Baral, M.M. Thawre, B. Ratna Sunil, R. Dumpala, A review on developing high-performance ZE41 magnesium alloy by using bulk deformation and surface modification methods. *J. Magnesium Alloys* **11**, 776-800 (2023). DOI: <https://doi.org/10.1016/j.jma.2023.03.001>
- [7] G.V. Jagadeesh, S. Gangi Setti, Experimental investigation and estimation of compressive residual stress of ball burnished rare

- earth based magnesium alloy. *Proc. Inst. Mech. Eng., Part E: J. Process* **238**, 351-362 (2022).
DOI: <https://doi.org/10.1177/09544089221144182>
- [8] M. Salahshoor, Y.B. Guo, Surface integrity of biodegradable Magnesium–Calcium orthopedic implant by burnishing. *J. Mech. Behav. Biomed. Mater.* **4**, 1888-1904 (2011).
DOI: <https://doi.org/10.1016/j.jmbbm.2011.06.006>
- [9] M. Uddin, C. Hall, V. Santos, R. Visalakshan, G. Qian, K. Vasilev, Synergistic effect of deep ball burnishing and HA coating on surface integrity, corrosion and immune response of biodegradable AZ31B Mg alloys. *Mater. Sci. Eng. C*, **118**, 111459 (2021).
DOI: <https://doi.org/10.1016/j.msec.2020.111459>
- [10] G.V. Jagadeesh, S. Gangi Setti, Surface integrity of ball burnished bioresorbable magnesium alloy. *Adv. Manuf.* **11**, 342-362 (2023).
DOI: <https://doi.org/10.1007/s40436-021-00387-6>
- [11] G.V. Jagadeesh, S. Gangi Setti, Tribological Performance Evaluation of Ball Burnished Magnesium Alloy for Bioresorbable Implant Applications. *J. Mater. Eng. Perform.* **31**, 1170-1186 (2022).
DOI: <https://doi.org/10.1007/s11665-021-06228-8>
- [12] G.V. Jagadeesh, S.G. Setti, Tribological Characterization of Ball Burnished Magnesium Alloy by Wear-Burnishing Maps, Wear Maps and Artificial Intelligence Technique. *Arabian J. Sci. Eng.* **48**, 3111-3131 (2023).
DOI: <https://doi.org/10.1007/s13369-022-07025-8>
- [13] A. Chaudhary, S.K. Baral, G. Tiwari, R. Dumpala, Finite element analysis of ball burnishing: evolution of residual stresses and surface profile in Ti-6Al-7Nb alloy. *Eng. Res. Express* **5**, 045015 (2023).
DOI: <https://dx.doi.org/10.1088/2631-8695/acfecb>
- [14] A.J. López, P. Rodrigo, B. Torres, J. Rams, Dry sliding wear behaviour of ZE41A magnesium alloy. *Wear* **271**, 2836-2844 (2011). DOI: <https://doi.org/10.1016/j.wear.2011.05.043>
- [15] D.K. Dwivedi, Sliding temperature and wear behaviour of cast Al–Si–Mg alloys. *Mater. Sci. Eng., A* **382**, 328-334 (2004).
DOI: <https://doi.org/10.1016/j.msea.2004.05.014>
- [16] F. Aydin, Y. Sun, Investigation of wear behaviour and microstructure of hot-pressed TiB₂ particulate-reinforced magnesium matrix composites. *Can. Metall. Q.* **57**, 455-469 (2018).
DOI: <https://doi.org/10.1080/00084433.2018.1478491>
- [17] S. Kailainathan, M. Ezhilan, S.V. Alagarsamy, C. Chanakyan, Investigations on Tribological Behaviour of Titanium Dioxide Particles Filled Al-0.6Fe-0.5Si Alloy Composite using TOPSIS Approach. *Arch. Metall. Mater.* **68**, 1429-1438 (2023).
DOI: <https://doi.org/10.24425/amm.2023.146209>
- [18] H. Chen, A.T. Alpas, Sliding wear map for the magnesium alloy Mg-9Al-0.9 Zn (AZ91). *Wear* **246**, 106-116 (2000).
DOI: [https://doi.org/10.1016/S0043-1648\(00\)00495-6](https://doi.org/10.1016/S0043-1648(00)00495-6)
- [19] S.A. selvan, S. Ramanathan, Dry sliding wear behavior of hot extruded ZE41A magnesium alloy. *Mater. Sci. Eng. A* **527**, 1815-1820 (2010).
DOI: <https://doi.org/10.1016/j.msea.2009.11.017>
- [20] S. Anbu selvan, S. Ramanathan, Dry sliding wear behavior of as-cast ZE41A magnesium alloy. *Mater. Des.* **31**, 1930-1936 (2010).
DOI: <https://doi.org/10.1016/j.matdes.2009.10.054>
- [21] M. Shen, X. Zhu, B. Han, T. Ying, J. Jia, Dry sliding wear behaviour of AZ31 magnesium alloy strengthened by nanoscale SiCp. *J. Mater. Res. Technol.* **16**, 814-823 (2022).
DOI: <https://doi.org/10.1016/j.jmrt.2021.12.048>
- [22] H.J. Hu, Z. Sun, Z.W. Ou, X.Q. Wang, Wear behaviors and wear mechanisms of wrought magnesium alloy AZ31 fabricated by extrusion-shear. *Eng. Fail. Anal.* **72**, 25-33 (2017).
DOI: <https://doi.org/10.1016/j.engfailanal.2016.11.014>
- [23] N.M. Chelliah, R. Kumar, H. Singh, M.K. Surappa, Microstructural evolution of die-cast and homogenized AZ91 Mg-alloys during dry sliding condition. *J. Magnesium Alloys* **5**, 35-40 (2017).
DOI: <https://doi.org/10.1016/j.jma.2017.02.001>
- [24] S.K. Baral, M.M. Thawre, B.R. Sunil, R. Dumpala, Temperature-dependent wear characteristics of ZE41 magnesium alloy under air and inert environments. *Materialwiss. Werkstofftech.* **54**, 1736-1744 (2023).
DOI: <https://doi.org/10.1002/mawe.202300042>
- [25] A.P. Murugesan, M. Mandal, P. Poddar, S. Bagui, Effect of Alloying Elements on the Dry Sliding Wear Characteristics of Gravity-Cast Mg-Sn Based Alloys. *J. Mater. Eng. Perform.* **32**, 10767-10782 (2023).
DOI: <https://doi.org/10.1007/s11665-023-07875-9>
- [26] A.-W. El-Morsy, Dry sliding wear behavior of hot deformed magnesium AZ61 alloy as influenced by the sliding conditions. *Mater. Sci. Eng. A*, **473**, 330-335 (2008).
DOI: <https://doi.org/10.1016/j.msea.2007.03.096>
- [27] M. Hu, Q. Wang, C. Chen, D. Yin, W. Ding, Z. Ji, Dry sliding wear behaviour of Mg–10Gd–3Y–0.4Zr alloy, *Mater. Des.* **42**, 223-229 (2012). DOI: <https://doi.org/10.1016/j.matdes.2012.05.051>